Theoretical and Experimental Chemistry, Vol. 50, No. 1, March, 2014 (Russian Original Vol. 50, No. 1, January-February, 2014)

CATALYTIC PROPERTIES OF NANOSIZED Cu/ZrO_2 SYSTEMS IN THE STEAM REFORMING OF BIOETHANOL

I. V. Deinega,[1] L. Yu. Dolgykh,[1] L. A. Staraya,[1] P. E. Strizhak,[1] E. M. Moroz,[2] and V. P. Pakharukova[2]

UDC 544.47:544.344

A size effect was found in the low-temperature steam reforming of bioethanol (15 vol. % ethanol in water) on copper catalysts supported on yttrium-stabilized zirconia: the specific rate of the conversion of ethanol into the key reforming product, acetaldehyde, is virtually independent on the mean diameter of the copper particles in the range 6-10 nm but drops significantly for particles with diameter 1-2 nm. Hypotheses for this observed effect are presented.

Key words: *temperature-programmed reduction, catalyst, copper, yttrium-stabilized zirconium dioxide, bioethanol, dehydrogenation, steam reforming.*

Copper-containing zirconia catalysts have attracted considerable attention in light of their high activity in important industrial processes for the manufacture of methanol from a mixture of hydrogen and carbon oxides, the low-temperature water-gas shift reaction, the steam reforming of methanol, and the selective catalytic reduction of nitrogen oxides by hydrocarbons. A number of studies have been devoted to copper catalysts in the reforming of ethanol [1-3], which have recently been intensively investigated in regard to the possibility of obtaining hydrogen and other valuable products from renewable resources.

The activity of copper catalysts depends on the crystal modification of ZrO_2 [4, 5]. The tetragonal zirconia modification is more efficient than the monoclinic modification in Ni/ZrO_2 catalysts for the steam reforming of ethanol to give hydrogen [6]:

$$C_2H_5OH + 3H_2O = 2CO_2 + 6H_2. \quad (1)$$

The catalytic properties of copper catalysts supported on amorphous, monoclinic, and tetragonal crystalline ZrO_2 in the conversion of ethanol to obtain acetaldehyde and ethyl acetate are related to the electronic properties of the supported copper particles and specific properties of the support [7].

In previous work [8], we studied the state and structure of the copper particles in yttrium-stabilized zirconia catalysts (3.4 mole % Y_2O_3, 96.4 mole % ZrO_2) obtained by coprecipitation of the hydroxides with subsequent microwave drying and

[1]L. V. Pisarzhevskii Institute of Physical Chemistry, National Academy of Sciences of Ukraine, Prospekt Nauky, 31, Kyiv 03028, Ukraine. E-mail: ldolgykh@inphyschem-nas.kiev.ua.

[2]Boreskov Institute of Catalysis, Siberian Branch, Prospekt Lavrentieva, 5, Novosibirsk 630090, Russian Federation. E-mail: emoroz@catalysis.ru.

Translated from Teoreticheskaya i Éksperimental'naya Khimiya, Vol. 50, No. 1, pp. 46-52, January-February, 2014. Original article submitted December 30, 2013; revision submitted February 6, 2014.

roasting. A small amount of copper atoms may be incorporated into the zirconia crystal lattice, while most of the active phase is formed as highly-dispersed chain clusters and copper oxide networks on the support surface. The clusters and particles, similar to bulk CuO, are not formed up to10 mass % copper content.

In the present work, we elucidated the effect of the copper content and specific surface of the support on reduction and the textural characteristics such as particle size, dispersity, specific surface, and the active phase of the metal of copper-containing yttrium-stabilized zirconia as well as the catalytic properties of the samples in the steam reforming of bioethanol.

EXPERIMENTAL

The catalysts were prepared by impregnation of the supports by an aqueous solution of $Cu(NO_3)_2 \cdot 3H_2O$ with subsequent drying at 80 °C and roasting in the air at 300 °C for 6 h. Laboratory samples of yttrium-stabilized zirconia (3 mole % Y_2O_3, 97 mole % ZrO_2) obtained by coprecipitation of the hydroxides and subsequent pulse wave treatment and roasting at 400 °C (YSZ_{400}) and 1000 °C (YSZ_{1000}) in order to vary the textural characteristics.*

The catalyst samples were characterized by X-ray diffraction (XRD), temperature-programmed hydrogen reduction (TPR), adsorption decomposition of N_2O with subsequent TPR, and nitrogen adsorption/desorption. These studies were carried out in accord with our previous procedure [9].

The catalytic properties of the samples were studied at atmospheric pressure in a quartz flow reactor with chromatographic monitoring of the starting and converted reaction mixtures [9]. The inlet rate for the liquid reagents (15 vol.% ethanol in water) was 0.03 cm^3/min. The inlet rate of the gas carrier (high-purity nitrogen) was 30 cm^3/min. Prior to the experiments, the catalyst was reduced *in situ* at 250 °C in a stream of 50% $H_2 + N_2$ (30 mL/min) for 2 h.

The ethanol conversion X (%) and selectivity relative to the carbon-containing products S_i (%) were calculated using the following formulas

$$X = \sum X_i = \frac{\sum n_i F_i}{2F^0_{C_2H_5OH}} \cdot 100, \tag{2}$$

$$S_i = \frac{n_i F_i}{\sum n_i F_i} \cdot 100 \tag{3}$$

where X_i is the conversion of ethanol to the i-th carbon-containing product, $F^0_{C_2H_5OH}$ and F_i are the flow rates of ethanol to the reactor and of the i-th carbon-containing product emerging from the reactor, respectively, mol/h, and n_i is the number of carbon atoms in the i-th carbon-containing product.

The selectivity relative to hydrogen S_{H_2} (%) was taken as 100% when six moles of H_2 are formed per mole of ethanol consumed in accord with stoichiometric Eq. (1):

$$S_{H_2} = \frac{F_{H_2}}{6(F^0_{C_2H_5OH} - F_{C_2H_5OH})} \cdot 100 = \frac{F_{H_2}}{3\sum n_i F_i} \cdot 100 \tag{4}$$

where F_{H_2} and $F_{C_2H_5OH}$ are the flow rates of hydrogen and ethanol emerging from the reactor, respectively, mol/h.

The rate of formation of hydrogen (R_{H_2}) was determined according to the flow rate of hydrogen emerging from the reactor F_{H_2} relative to the catalyst sample m_{cat}:

$$R_{H_2} = F_{H_2}/m_{cat}. \tag{5}$$

---

*The samples were provided by T. E. Konstantinova of the Donetsk Institute for Physics and Engineering named after O. O. Galkin, National Academy of Sciences of Ukraine.

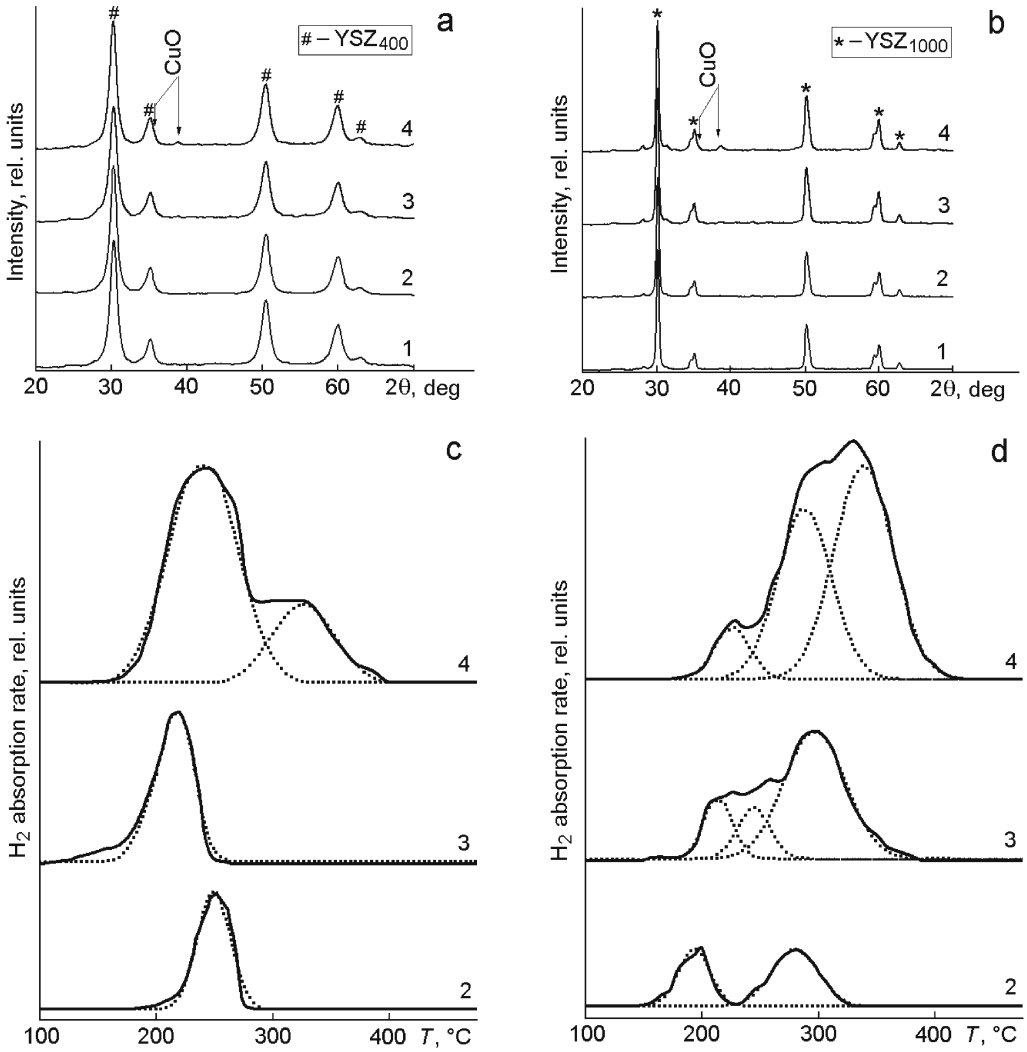

Fig. 1. Diffraction patterns for nCu/YSZ$_{400}$ (a) and nCu/YSZ$_{1000}$ (b); curves for the temperature-programmed reduction of catalysts nCu/YSZ$_{400}$ (c) and nCu/YSZ$_{1000}$ (d) with different copper contents n: 1) 0, 2) 2, 3) 5, and 4) 10 mass %.

RESULTS AND DISCUSSION

Figure 1 shows diffraction patterns for supports YSZ$_{400}$ and YSZ$_{1000}$ and the derived copper-containing catalysts with various copper contents (nCu/YSZ, n = 2, 5, and 10 mass % Cu) as well as curves for the temperature-programmed reduction of the samples. The specific surface of YSZ$_{1000}$ and YSZ$_{400}$ from the nitrogen adsorption/desorption data was 17 and 128 m^2/g, respectively.

Analysis of the diffraction patterns of YSZ$_{400}$ and nCu/YSZ$_{400}$ (Fig. 1a) indicated that the YSZ$_{400}$ support has unit cell parameters a = 0.3629 nm, c = 0.5106 nm ($c/\sqrt{2a}$ = 0.995) and forms crystals with fluorite structure. The diffraction patterns of YSZ$_{400}$ and nCu/YSZ$_{400}$ studied in this work are analogous to the patterns obtained in our previous work [8]. Weak diffraction peaks for massive CuO were observed only for 10Cu/YSZ$_{400}$ (the positions of the lines at 2θ = 35.5° and 38.6° characteristic for CuO are shown by arrows).

The XRD results indicated that the tetragonal zirconia phase predominates for YSZ$_{1000}$ and nCu/YSZ$_{1000}$ with unit cell parameters a = 3.608 Å, c = 5.167 Å, $c/\sqrt{2a}$ = 1.013 (Fig. 1b). The samples also contain a trace of monoclinic zirconia

TABLE 1. Concentration of Copper Atoms on the Surface of the Support Cu/S_{sp}, Temperatures for Reduction Maxima (T) and the Amount of Absorbed Hydrogen (m) in the Temperature-Programmed Reduction (TPR) of Cu/YSZ Catalysts

Catalyst	Cu/S_{sp}, atom/nm^2	T_i, °C				m_i, mmol/g			
		$T_{\beta1}$	$T_{\beta2}$	$T_{\beta3}$	T_{γ}	$m_{\beta1}$	$m_{\beta2}$	$m_{\beta3}$	m_{γ}
$2Cu/YSZ_{400}$	1.5	–	247	–	–	–	0.30	–	–
$5Cu/YSZ_{400}$	3.7	–	221	–	–	–	0.83	–	–
$10Cu/YSZ_{400}$	7.3	–	240	–	340	–	1.22	–	0.40
$2Cu/YSZ_{1000}$	11.1	198	–	275	–	0.08	–	0.14	–
$5Cu/YSZ_{1000}$	27.4	226	256	300	–	0.10	0.09	0.45	–
$10Cu/YSZ_{1000}$	55.3	–	225	290	338	–	0.11	0.55	0.75

(<5 mass %). In catalysts with copper content up to 5 mass % inclusive, no peaks corresponding to individual copper compounds were found. Increasing the copper content to 10 mass % leads to the appearance of reflections in the diffraction pattern related to the bulk copper oxide phase.

The TPR curves for the Cu/YSZ samples shown in Fig. 1c,d show several overlapping peaks. The peaks were separated for quantitative analysis using the Gaussian function and integrated to determine their individual areas. Table 1 summarizes the data on the temperature maximum of the reduction rate and amount of absorbed hydrogen for the Cu/YSZ samples with different amounts of copper and specific surface of the support. The indices β1, β2, and β3 indicate the reduction peaks of dispersed cupric oxide peaks, while the index γ indicates reduction of bulk CuO particles, which is discussed below. For the same copper content, the values of Cu/S_{sp}, giving the ratio of the amount of copper atoms per unit of surface area of the support for $n Cu/YSZ_{400}$ samples on the support with high specific surface and $n Cu/YSZ_{1000}$ samples on the support with low specific surface, differ significantly. The values of Cu/S_{sp} for YSZ_{400} do not exceed 7.3 atom/nm^2, which is lower than the dispersion capacity of the support, which is 8.6 Cu^{2+} ion/nm^2 for tetragonal zirconia and characterizes the state when all the possible vacant sites on the zirconia surface are occupied by cupric ions [10]. For catalysts derived from YSZ_{1000}, the values of Cu/S_{sp} range from 11.1 to 55.3 atom/nm^2, which is considerably greater than the dispersion capacity of the support.

Analysis of the reduction curves for Cu/YSZ_{400} shows that there is one peak with maximum reduction temperature $T_{\beta2}$ = 247 °C for $2Cu/YSZ_{400}$ with Cu/S_{sp} = 1.5 atom/nm^2 (Fig. 1c, curve 2). The TPR curve for $5Cu/YSZ_{400}$ (Cu/S_{sp} = 3.7 atom/nm^2) has a peak with $T_{\beta2}$ = 221 °C (Fig. 2c, curve 3), while the $10Cu/YSZ_{400}$ sample (Cu/S_{sp} = 7.3 atom/nm^2) has a pronounced peak at $T_{\beta2}$ = 240 °C and a shoulder at T_{γ} = 340 °C (Fig. 1c, curve 4).

The TPR curves for the Cu/YSZ_{1000} samples have more complex structure. Two separate peaks are seen for $2Cu/YSZ_{1000}$ (Cu/S_{sp} = 11.1 atom/nm^2, Fig. 1d, curve 2) with maximum reduction temperatures $T_{\beta1}$ = 198 °C and $T_{\beta3}$ = 275 °C. Three overlapping peaks were recorded for the catalyst containing 5 mass % copper (Cu/S_{sp} = 27.4 atom/nm^2) with observed maximum reduction temperatures $T_{\beta1}$ = 226 °C, $T_{\beta2}$ = 256 °C, and $T_{\beta3}$ = 300 °C (Fig. 1d, curve 3). Peaks with $T_{\beta2}$ = 225 °C, $T_{\beta3}$ = 290 °C, and T_{γ} = 338 °C were found for $10Cu/YSZ_{1000}$ (Cu/S_{sp} = 55.3 atom/nm^2, Fig. 1d, curve 4).

The finding of several reduction peaks for the copper catalysts supported on zirconia is in accord with previous reports [5, 10-12] and may indicate the existence of several types of copper oxide particles on the support surface. The value of T_i for the highest temperature peak is close to the TPR maximum of massive CuO under the same conditions, which was established in separate experiments. Thus, the peaks with T_{γ} = 338 °C (for $10Cu/YSZ_{1000}$) and T_{γ} = 340 °C (for $10Cu/YSZ_{400}$) may be assigned to the reduction of massive CuO particles, which is supported by the XRD data showing diffraction peaks for the CuO phase in these samples. We may propose that the TPR peaks with temperature maxima in the range 198-300 °C (β-peaks)

TABLE 2. Temperatures for Reduction Maxima (T_s) and Amount of Absorbed Hydrogen (m_s) in the Temperature-Programmed Reduction of after Prior Oxidation of the Metallic Copper Surface by N_2O (*s*-TPR), Dispersity D_{Cu}, Specific Surface S_{Cu}, Mean Particle Diameter d_{Cu} and Total Surface S of Reduced Copper Particles in Cu/YSZ Catalysts according to *s*-TPR Data

Catalyst	T_s, °C	m_s, mmol/g	D_{Cu}, %	S_{Cu}, m^2/g_{Cu}	d_{Cu}, nm	S, m^2/g_{cat}
$2Cu/YSZ_{400}$	200	0.15	96	615	1	15.3
$5Cu/YSZ_{400}$	197	0.33	85	543	1	27.2
$10Cu/YSZ_{400}$	211	0.42	53	336	2	33.6
$2Cu/YSZ_{1000}$	179	0.06	38	246	3	4.9
$5Cu/YSZ_{1000}$	195	0.07	18	116	6	5.8
$10Cu/YSZ_{1000}$	227	0.09	10	70	10	7.0

characterize the reduction of highly dispersed copper oxide particles and copper oxide microcrystallites with different extent of interaction with ZrO_2 [10, 12].

The amount of absorbed hydrogen for the nCu/YSZ_{1000} catalysts is somewhat less than the amount corresponding to the complete reduction of the CuO particles (H_2/CuO = 0.8-0.9), while the H_2/CuO ratio is 1.0-1.1 for the series of nCu/YSZ_{400} samples.

The textural characteristics of the particles of reduced copper on the support surface as well as the reactivity of these particles permit us to evaluate the analysis of the temperature-programmed reduction curves, obtained after oxidation of the metallic copper surface using N_2O (*s*-TPR). Table 2 gives the temperatures for the maximum reduction rate T_s and the amount of absorbed hydrogen m_s obtained during *s*-TPR as well as the textural characteristics of the reduced copper particles on the YSZ surface calculated from the *s*-TPR curves.

Upon summarizing the data for the reduction of nCu/YSZ samples taking account our previous results [8], we may conclude that mostly copper oxide nanoclusters with chain structure on yttrium-stabilized zirconia with low Cu/S_{sp} ratios (1.5-3.7 atom/cm^2) are formed. The reduction of these nanoclusters ($T_{\beta 2}$ = 221-247 °C) leads to the formation of active phase particles with mean diameter ~1 nm. The specific copper surface is 543-615 m^2/g depending on Cu/S_{sp}. For Cu/$S_{sp} \geq$ 7 atom/nm^2, highly dispersed cupric oxide particles are formed with $T_{\beta i}$ in the range 198-256 °C along with CuO microcrystallites ($T_{\beta 3}$ = 275-300 °C) and bulk CuO particles (T_{γ} = 338-340 °C). Table 1 shows the fraction of these types of particles depends on the copper content and specific surface of the support. The reductive treatment of nCu/YSZ samples with Cu/$S_{sp} \geq 7$ atom/nm^2 leads to the formation of copper nanoparticles with diameter 2-10 nm and specific surface from 240 to 70 m^2/g depending on the value of Cu/S_{sp}. In the case of low copper content, its highly dispersed particles have higher reactivity as indicated by a lower value of T_s (Table 2). The reactivity of the Cu particles decreases somewhat with increasing contribution of the massive CuO particles to formation of the active phase, which is observed for the samples with 10 mass % copper content. This is indicated by the shift of T_s toward higher temperatures. The similarity of the reduction temperatures of $5Cu/YSZ_{400}$ and $5Cu/YSZ_{1000}$ in the *s*-TPR process may indicate similar reactivity of the reduced copper particles in these catalysts.

Figure 2 illustrates the catalytic properties of Cu/YSZ samples in the steam reforming of bioethanol. The high selectivity relative to acetaldehyde and finding hydrogen in the mixture converted at T < 325 °C indicate the predominant dehydrogenation of ethanol:

$$C_2H_5OH = CH_3CHO + H_2. \quad (6)$$

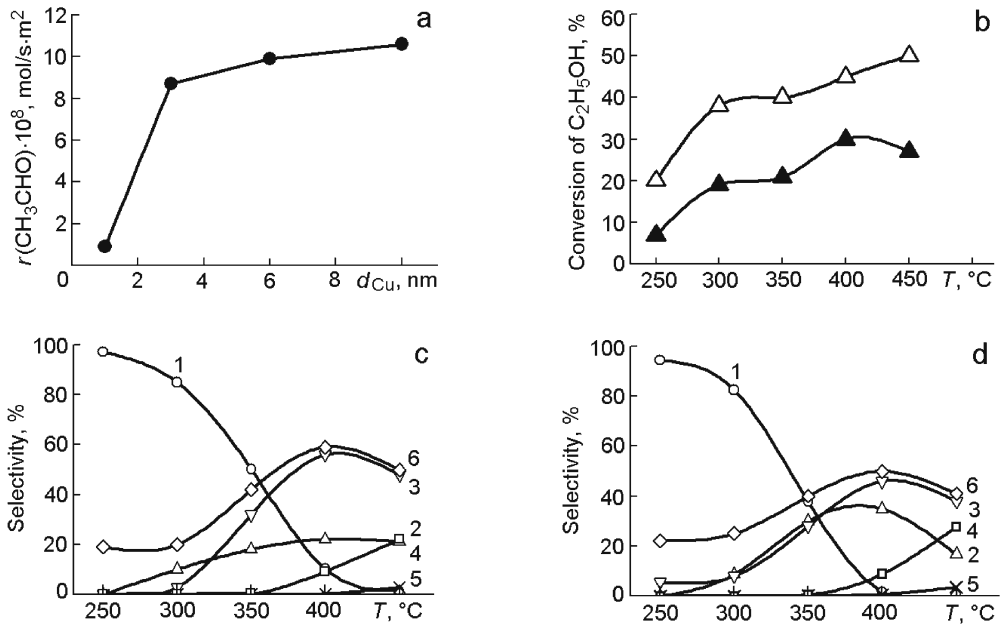

Fig. 2. Specific rate of the conversion of ethanol to acetaldehyde $r(CH_3CHO)$ depending on the mean diameter of the copper particles d_{Cu} (a), ethanol conversion on $5Cu/YSZ_{1000}$ (Δ) and $5Cu/YSZ_{400}$ (▲) (b), formation selectivity of the products of the steam reforming of ethanol on $5Cu/YSZ_{1000}$ (c) and $5Cu/YSZ_{400}$ (d) at different temperatures: 1) CH_3CHO, 2) CH_3COCH_3, 3) CO_2, 4) C_2H_4, 5) CH_4, and 6) H_2.

The specific rate of acetaldehyde formation (the key product of the steam reforming of bioethanol) $r(CH_3CHO)$ at 300 °C hardly depends on the particle diameter in the range 6-10 nm (Fig. 2a). This result agrees with our previous data for copper catalysts with monoclinic ZrO_2 [10]. Reducing the particle diameter to less than 3 nm leads to a decrease in $r(CH_3CHO)$, indicating the existence of size effect. We should note that this effect is seen for $Cu/S_{sp} < 7$ atom/nm^2, which is less than the dispersion capacity of zirconia. The XRD and TPR data indicate that formation of massive cupric oxide is not observed in this region and the formation of clusters of reduced active phase atoms occurs most likely from chain oxide species. An increase in Cu/S_{sp} enhances the probability of formation of larger disperse cupric oxide particles and cupric oxide microcrystallites and, as a consequence, an increase in the size of the reduced metallic phase particles. The $n Cu/YSZ_{1000}$ catalysts (n = 2, 5, 10 mass %), containing such particles, have higher specific catalytic activity. The observed dependence may be explained in the framework of the differentiation of small particles according to whether these particles include clusters with an unformed surface and dispersed particles with a formed surface [13]. Thus, the decrease in the catalytic activity of the samples with cluster-size active phase copper particles (~1 nm) is most likely related to features of formation of the surface of such particles.

Figure 2b gives a comparison of the ethanol conversion X at different temperatures for catalysts with the same copper content $5Cu/YSZ_{1000}$ and $5Cu/YSZ_{400}$. Upon an increase in the temperature from 250 to 450 °C, the ethanol conversion on $5Cu/YSZ_{1000}$ increases from 21.8 to 51.8%, while the value of X for $5Cu/YSZ_{400}$ increases from 5.8 to 26.2%, which is much less than the values of X for the YSZ_{1000} samples. We may propose that the lack of a sufficient quantity of dispersed cupric oxide particles with a formed surface on the surface of $5Cu/YSZ_{400}$, which are then involved in the formation of the reduction active phase nanoparticles, may account for the lower catalytic activity of this catalyst in comparison with $5Cu/YSZ_{1000}$.

Comparison of the data given in Fig. 2c and Fig. 2d shows 99% selectivity relative to acetaldehyde at T = 250 °C on the $5Cu/YSZ_{1000}$ catalyst, while this value is only 93% on $5Cu/YSZ_{400}$ and decreases with increasing temperature. We concurrently observed an increase in the selectivity relative to acetone to 22.3% on $5Cu/YSZ_{1000}$ (T = 450 °C) and 32.6% (T = 350 °C) with a subsequent decrease to 13.8% on $5Cu/YSZ_{400}$. For both catalysts at T > 350 °C, we observed an

increase in selectivity relative to methane from 6 to 9% and also in selectivity relative to ethylene from 22.4 to 25.3% for $5Cu/YSZ_{1000}$ and $5Cu/YSZ_{400}$, respectively.

The observed products suggest that the initial conversion of ethanol proceeds predominantly by means of the dehydrogenation of this alcohol to give acetaldehyde (reaction (6)). At elevated temperatures, acetaldehyde undergoes further transformation with steam, leading to the formation of hydrogen, carbon dioxide, acetone, and methane in the products:

$$CH_3CHO + H_2O = CH_4 + CO_2 + H_2, \quad (7)$$

$$2CH_3CHO + H_2O = CH_3COCH_3 + CO_2 + 2H_2. \quad (8)$$

The formation of ethylene is the result of the dehydrogenation of ethanol with involvement of the acid sites of the support [14]:

$$C_2H_5OH = C_2H_4 + H_2O. \quad (9)$$

Under the conditions studied, the $5Cu/YSZ_{1000}$ catalyst has higher selectivity relative to CO_2 (54.8% at 400 °C). The selectivity relative to hydrogen is 58.9% on $5Cu/YSZ_{1000}$ and 48.4% on $5Cu/YSZ_{400}$ at 400 °C. The rate of hydrogen formation is 4.3 and 2.3 mmol/h·g_{cat} on $5Cu/YSZ_{1000}$ and $5Cu/YSZ_{400}$, respectively. These findings indicate the high rate of steam reforming reactions on $5Cu/YSZ_{1000}$. The high selectivity of $5Cu/YSZ_{1000}$ relative to CO_2 probably is due to the higher mobility of support oxygen, which facilitates the oxidation of the carbon-containing intermediates on the path to CO_2 by oxygen on the zirconia surface [15]. This is favored by the higher concentration of oxygen vacancies per unit of support surface, which are formed upon the introduction of yttrium oxide as a stabilizer and the possible insertion of cupric ions into the zirconia crystal lattice as well as the formation of the support at high temperatures.

Thus, our studies have shown a size effect in the dehydrogenation of ethanol to give acetaldehyde on copper catalysts supported on yttrium-stabilized zirconia. The differences in the activity of the catalysts are probably due to features of the surfaces of the clusters and dispersed species of copper in the samples. The enhanced selectivity of the catalysts made with yttrium-stabilized zirconia (YSZ) roasted at 1000 °C (S_{sp} = 17 m^2/g) in the steam reforming of bioethanol relative to YSZ roasted at 400 °C (S_{sp} = 128 m^2/g) may be related to the higher mobility of oxygen in the support.

REFERENCES

1. M. Ni, D. Y. C. Leung, and M. K. H. Leung, *Int. J. Hydrogen Energy*, **32**, 3238-3247 (2007).
2. P. D. Vaidya and A. E. Rodrigues, *Chem. Eng. J.*, **117**, 39-49 (2006).
3. A. Haryanto, S. Fernando, N. Murali, and S. Adhikari, *Energy Fuels*, **19**, 2098-2106 (2005).
4. K. T. Jung and A. T. Bell, *Catal. Lett.*, **80**, 63-68 (2002).
5. R.-X. Zhou, X.-Y. Jiang, J.-X. Mao, and X.-M. Zheng, *Appl. Catal. A*, **162**, 213-222 (1997).
6. M. Benito, R. Padilla, L. Rodriguez, et al., *J. Power Sources*, **169**, 167-176 (2007).
7. A. G. Sato, D. P. Volanti, D. M. Meira, et al., *J. Catal.*, **307**, 1-17 (2013).
8. V. P. Pakharukova, E. M. Moroz, V. V. Kriventsov, et al., *J. Phys. Chem. C*, **113**, 21368-21375 (2009).
9. L. Yu. Dolgikh, Yu. I. Pyatnitskii, S. I. Reshetnikov, et al., *Teor. Éksp. Khim.*, **47**, No. 5, 309-314 (2011). [*Theor. Exp. Chem.*, **47**, No. 5, 324-330 (2011) (English translation).]
10. Z. Liu, M. Amiridis, and Y. Chen, *J. Phys. Chem. B*, **109**, 1251-1255 (2005).
11. W. P. Dow, Y.-P. Wang, and T.-J. Huang, *J. Catal.*, **160**, 155-170 (1996).
12. Z.-Y. Ma, C. Yang, W. Wei, et al., *J. Mol. Catal. A*, **231**, 75-81 (2005).
13. K. I. Patrylak, L. K. Patrylak, and S. V. Konovalov, *Teor. Éksp. Khim.*, **49**, No. 1, 32-36 (2013). [*Theor. Exp. Chem.*, **49**, No. 1, 35-39 (2013) (English translation).]
14. Y. Zhao, W. Li, M. Zhang, and K. Tao, *Catal. Commun.*, **3**, 239-245 (2002).
15. J. D. A. Bellido and E. M. Assaf, *J. Power Sources*, **177**, 24-32 (2008).